Transient Multiphase Model for the High-Temperature Thermal Treatment of Wood

R. Younsi, D. Kocaefe, S. Poncsak, and Y. Kocaefe
Dept. of Applied Sciences, University of Quebec at Chicoutimi, Chicoutimi, Québec, Canada G7H 2B1

DOI 10.1002/aic.10860
Published online April 20, 2006 in Wiley InterScience (www.interscience.wiley.com).

The hygrothermal behavior of wood at high temperature is analyzed, taking into account all the phases present such as wood, liquid water in free and bound forms, and water vapor. The moisture transport phenomenon includes water vapor convection and diffusion along with capillary water convection in the pores of the particle as well as bound water diffusion in the solid wood. Local thermodynamic equilibrium is assumed, which is represented by a sorption isotherm that relates the moisture contents in the solid and gas phases. The equations of the model were solved numerically using the commercial software Femlab® for the temperature and the moisture content profiles. The mathematical model predictions were compared with the experimental data and a reasonably good agreement was obtained. A parametric study was also carried out to determine the effects of several parameters such as heating rate, initial moisture content, and the sample thickness on the temperature and moisture content distributions within the samples during heat treatment. © 2006 American Institute of Chemical Engineers *AIChE J,* 52: 2340–2349, 2006
Keywords: mathematical modeling, heat and moisture transfer, high-temperature wood treatment, validation of mathematical model

Introduction

Wood continues to be the principal raw material for a large number of products in construction and furniture industries, although other competitive materials such as metals and plastics are also available. To ensure a suitable and usable end product and to prevent undesirable biochemical reactions and microbiological growth, most of the moisture present in wood must be removed. In most industrial drying operations, heat is supplied externally to wood by air or superheated steam to evaporate the moisture. During these conventional heat treatment processes (drying), the wood is heated to about 120°C and the water is removed by evaporation. Full descriptions of the moist air and superheated steam drying models are given elsewhere.[1-4]

The high-temperature treatment of wood is different from that of conventional drying. This technique offers an alternative to the chemical treatment of wood, which uses traditional oil (creosote and pentachloro-phenol) and chromated copper arsenate (CCA). These chemicals are toxic and, thus, harmful when they are released into the environment. During the high-temperature treatment process, the wood species with different moisture contents are heated slowly up to 200–230°C in a hot inert gas atmosphere. This treatment reduces the hydrophilic behavior of wood by modifying the chemical structure of some of its components.

Several physical mechanisms contribute to the migration of moisture in wood during its removal. In a porous solid medium containing free water, bound water, vapor, and air or any other gas, the moisture transport through the medium can be in the form of either diffusion or capillary flow driven by individual or combined effects of the moisture, temperature, and pressure gradients. The predominant mechanisms that control the moisture transfer depend on the hygroscopic nature and properties of the materials as well as the heating conditions.

In the literature, a number of investigations have been undertaken by various researchers[5-7] to study the heat and moisture transfer in porous materials. Luikov[5] developed a set of

Correspondence concerning this article should be addressed to R. Younsi at ryounsi@uqac.ca.

coupled partial differential equations (PDEs) to describe the heat and mass transport in capillary porous media. It was assumed that the moisture transfer is similar to the heat transfer. It was indicated that the capillary transport taking place in the pores results in moisture and temperature gradients. Lewis et al.[8] and Malan and Lewis[9] showed that the finite element numerical solution procedures are suitable to solve the highly nonlinear equations describing such drying systems. It is difficult to represent the moisture transfer in porous media in a satisfactory way using purely diffusive, uncoupled heat and mass transfer models without taking into account the phase changes and related thermal effects that occur.[10] In comparison with others, Whitaker's model[7] is more comprehensive and rigorously formulated because it derives the macroscopic equations through a volume-averaging technique at a control point and considers in great detail the transport mechanisms of moisture and energy within the media.

In the present study, a three-dimensional (3-D) mathematical model for the high-temperature thermal treatment of wood has been developed to calculate the heat and mass transfer during the process. The model is based on the approach reported by Whitaker,[7] Bear,[11] and Hassanizadeh and Gray.[12] Three moisture phases are taken into account: free (liquid) water, bound water, and water vapor. An effort was made to consider the moisture and/or temperature dependency of the thermodynamic, physical, and transport properties. A large number of experiments were performed under different operating conditions and the data were compared with the model predictions. To date, no high-temperature thermal wood treatment model that considers all the phases involved has been reported in the literature.

Mathematical modeling allows a better understanding of the interacting mechanisms involved in a complex production process. Knowledge of moisture and temperature profiles within the wood and understanding of the fundamental mechanisms during the heating process are essential for process design (optimization, reduction of treatment time), quality control, operating and handling practices, and energy savings.

Mathematical Model

The high-temperature thermal treatment of wood involves the simultaneous transport of heat and mass within three phases (wood, liquid water including free and bound water, and vapor). In the formulation of the mathematical model, the main transport mechanisms have been identified and the equations were written to describe the system. The problem considers a sample of wood exposed to convective heating in an inert atmosphere. Figure 1 shows the geometry and the mesh of the sample.

The governing equations were derived at the macroscopic level. Variables used in this study are averaged values over a control volume. This approach was first proposed by Whitaker[7] and, since then, has been widely used in heat and mass transfer studies related to the drying of porous media.[13]

Assumptions

The assumptions used in the model are as follows:

- The porous system is 3-D
- The enthalpy for all three phases is a linear function of temperature

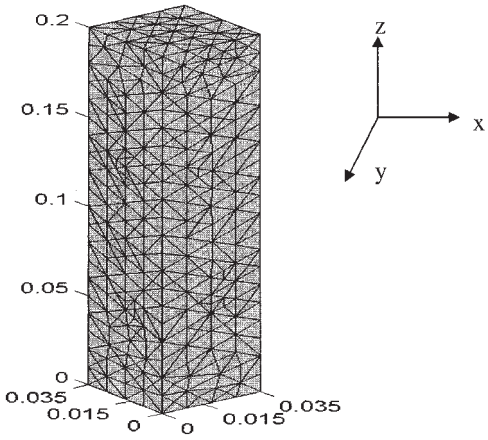

Figure 1. Representation of the geometry and the mesh.

The numbers indicate the dimensions in meters.

- The transport of free water is governed by the generalized Darcy's law
- The bound-water transport is driven by chemical potential difference[14]
- The liquid water is incompressible
- The solid, liquid, and gas phases are continuous
- The vapor phase obeys the ideal gas law
- The local vapor pressure as a function of moisture content and temperature can be estimated using sorption isotherms
- Shrinkage and gravity are neglected, and no degradation of solid occurs

Governing equations

Conservation of Mass. The conservation of mass requires that the rate of change of water mass inside a control volume is equal to the net flux of water leaving from the surface of the control volume, thus:

$$-\rho_d \frac{\partial M}{\partial t} = \nabla \cdot \mathbf{J} = \frac{\partial J_x}{\partial x} + \frac{\partial J_y}{\partial y} + \frac{\partial J_z}{\partial z} \tag{1}$$

where $\mathbf{J}$ is the total mass flux vector, ρ_d is the dry wood density, and M is the water moisture content per unit mass of dry wood.

The total mass flux can be written as

$$\mathbf{J} = \mathbf{J_v} + \mathbf{J_b} + \mathbf{J_f} \tag{2}$$

where $\mathbf{J_v}$, $\mathbf{J_b}$, and $\mathbf{J_f}$ are the fluxes of moisture arising from water vapor, bound water, and free water, respectively.

Conservation of Energy

$$\frac{\partial}{\partial t}(\rho_a u_a + \rho_v u_v + \rho_b u_b + \rho_f u_f + \rho_d u_d) + \nabla \cdot (\mathbf{J}_a h_a + \mathbf{J}_v h_v + \mathbf{J}_b h_b + \mathbf{J}_f h_f) = \nabla(k \nabla T) \tag{3}$$

where ρ, u, h, and k are the density, specific internal energy, specific enthalpy, and thermal conductivity, respectively. The subscript a is used for air (or gas), v for water vapor, b for bound water, f for free water, and d for dry wood. The gas

present in wood is immobile with a negligible heat capacity; therefore, the two terms representing the contributions of gas $(\partial/\partial t)\rho_a u_a$ and $\nabla \cdot \mathbf{J}_a h_a$ are neglected.

Before writing the conservations of mass and energy in their final forms, expressions for the fluxes appearing in Eq. 2 will be elaborated.

Vapor Flux. The flow of water vapor in the porous body of wood occurs according to two mechanisms. First, the vapor flows because of the total pressure gradient. Because of the small size of the pores, the flow is laminar in nature and the vapor flux can be expressed by Darcy's law. Second, the vapor migrates by diffusion as a result of its concentration (partial pressure) gradient. In the present work, there is no bulk flow of the humid gas within the wood because the total pressure gradient is assumed to be negligibly small. Therefore, the vapor diffusion is expressed by Fick's law:

$$\mathbf{J}_v = -\frac{m_v D_{eff}}{RT}\nabla P_v \tag{4}$$

where m_v is the molar mass of vapor, R is the ideal gas constant, and P_v is the partial vapor pressure of water, which is calculated using the following empirical correlation obtained by Moyne[15]:

$$P_v = P_{sv}(T)\Psi(M, T) \tag{5}$$

P_{sv} (the saturation partial pressure of water vapor) and Ψ (a coefficient) are calculated from the following empirical relationships:

$$P_{sv} = \exp(25.5058 - 5204.9/T)$$

$$\Psi(M, T) = \exp[(17.884 - 0.1423T + 23.63 \times 10^{-5}T^2) \times (1.0237 - 67.4 \times 10^{-5}T)^{92M}] \tag{6}$$

Bound Water Flux. The bound water diffusion occurs mostly when the moisture content is below the fiber saturation point (FSP) and is driven by the chemical potential difference. The flux of bound water can be expressed by[14]

$$\mathbf{J}_b = -\frac{D_b}{m_v}\left\{-\left[187 + 35.1\ln\left(\frac{T}{298.15}\right) - 8.314\ln\left(\frac{P_v}{101{,}325}\right)\right]\nabla T + 8.314\frac{T}{P_v}\nabla P_v\right\} \tag{7}$$

The diffusion coefficient of bound water is found using[16] $D_b = \exp(-9.9 + 9.8M_b - 4300/T)$.

Liquid Water Flux. The movement of free water, which occurs only for moisture contents higher than FSP, arises from capillarity between liquid and vapor phases within the cell lumens of the wood. The flux of this phase is thus obtained from Darcy's law as

$$\mathbf{J}_f = -\frac{K_l\rho_l}{\mu_l}\nabla P_l = -\frac{K_l\rho_l}{\mu_l}\nabla P_c \tag{8}$$

where P_c is the capillary pressure; ρ_l and μ_l are the density and viscosity of the liquid water. Spolek and Plumb[17] assumed that the capillary pressure is only a function of saturation as follows:

$$P_c = \alpha S^{-\beta} \tag{9}$$

where $\alpha = 1 \times 10^4$ and $\beta = 0.61$. The saturation of wood (S) is calculated by

$$S = \frac{M - M_{\mathrm{FSP}}}{M_{\max} - M_{\mathrm{FSP}}} \tag{10}$$

where M_{FSP} is the moisture content at fiber saturation point and $M_{\max}$ is the moisture content if the entire void within the wood structure was filled with water. This is expressed in terms of the dry wood void space ε_d, dry wood density ρ_d, and the density of water ρ_l as

$$M_{\max} = \varepsilon_d\frac{\rho_l}{\rho_d} \tag{11}$$

where the dry wood void space is given by

$$\varepsilon_d = \left(1 - \frac{\rho_d}{1500}\right) \tag{12}$$

M_{FSP} is the moisture content at the FSP, defined as[16]

$$M_{\mathrm{FSP}} = 0.57315 - 0.001T \tag{13}$$

Combining the above equations, the free water flux may be expressed as

$$\mathbf{J}_f = -\frac{K_l\rho_l}{\mu_l}\nabla P_l = -\frac{\alpha\beta K_l\rho_l(M_{\max} - M_{\mathrm{FSP}})^{\beta}}{\mu_l(M - M_{\mathrm{FSP}})^{(1+\beta)}}\nabla M \tag{14}$$

Substituting the expressions for the fluxes of different moisture phases in Eqs. 1 and 2, the mass and energy balances can be written as

Mass Balance

$$\rho_d\frac{\partial M}{\partial t} = \nabla(D_M\nabla M + D_T\nabla T) \tag{15}$$

Energy Balance

$$(\rho C_p)_{eff}\frac{\partial T}{\partial t} = \nabla(k_M\nabla M + k_{eff}\nabla T) \tag{16}$$

The coefficients D_M, D_T, $(\rho C_p)_{eff}$, k_{eff}, and k_M are positive coefficients and their expressions are given in Appendix A. The properties of liquid water and vapor are taken as a function of temperature. These correlations, obtained by fitting polynomials to the steam table data, are presented in Appendix B.[18] The

resulting coupled heat- and mass-transfer equations are nonlinear.

Initial and boundary conditions

The initial conditions can be written as

$$\left.\begin{aligned} M(x, y, z, 0) &= M_0 \\ T(x, y, z, 0) &= T_0 \end{aligned}\right\} \qquad \text{at } t = 0 \tag{17}$$

The boundary conditions at the surfaces are obtained from the heat and mass transfer correlations between the sample surface and the surrounding gas. For the mass transfer at the surfaces[9]

$$J_n = h_m \rho_v (M - M_{eq}) \tag{18}$$

where h_m is the mass-transfer coefficient, ρ_v is the water vapor density, and M_{eq} is the equilibrium moisture content obtained from the Hailwood–Horrobin equation adopted for wood by Simpson and Tenwold[19] (see Appendix C).

The heat balance at the surface requires that

$$[k_{eff} \nabla T]\vec{n} = h(T - T_g) + \Delta h_v J_n \tag{19}$$

where Δh_v is the latent heat of vaporization and h is the heat-transfer coefficient. The values of convective mass- and heat-transfer coefficients (h_m and h) at each point on the surfaces are found from the following expressions for laminar flow,[20] respectively:

$$\mathrm{Sh} = \frac{h_m L}{D} = 0.664\ \mathrm{Re}^{0.5}\mathrm{Sc}^{0.33}$$

$$\mathrm{Nu} = \frac{hL}{k} = 0.664\ \mathrm{Re}^{0.5}\mathrm{Pr}^{0.33} \tag{20}$$

where Sh is the Sherwood number, Re is the Reynolds number, Sc is the Schmidt number, Nu is the Nusselt number, Pr is the Prandtl number, and L is the length of the sample.

Thermophysical properties of wood

The density (ρ), specific gravity (G_m), specific heat (C_p), and thermal conductivities in the x, y, and z directions (k_x, k_y, k_z) of moist wood are calculated using the relations proposed by Simpson and Tenwold[19] and Siau[17]:

$$\rho = 1000 \times G_m(1 + M/100) \qquad (\mathrm{kg/m^3}) \tag{21}$$

$$C_p = (C_{p0} + 0.01 C_{pw})/(1 + 0.01M) + A_c \qquad (\mathrm{kJ\ kg^{-1}\ K^{-1}}) \tag{22}$$

where M is moisture content (%), C_{pw} is the heat capacity of water (4.19 kJ kg^{-1} K^{-1}), C_{p0} is the heat capacity of dry wood, and A_c is a parameter that is a function of moisture content and temperature. C_{p0} and A_c are given, respectively, as

$$C_{p0} = 0.1031 + 0.003867T \qquad (\mathrm{kJ\ kg^{-1}\ K^{-1}}) \tag{23}$$

Table 1. Model Input Parameters Used in Numerical Investigation

Parameter	Unit	Value
G_m	—	0.66
h	W m^{-2} K^{-1}	15
h_m	m s^{-1}	1.6×10^{-5}
M_0	% (kg/kg)	7–30
K_1	m^2	5×10^{-16}
m_v	kg mol^{-1}	0.018
T_0	K	298
R	J mol^{-1} K^{-1}	8.314
ρ_d	kg m^{-3}	660

$$A_c = M(-0.06191 + 2.36 \times 10^{-4} T - 1.33 \times 10^{-4} M) \tag{24}$$

The thermal conductivity of wood in the longitudinal direction is approximately two times greater than that in the transversal or radial directions as reported in the literature.[16,21] The thermal conductivities in different directions are

$$(k_z = 2.5k_x = 2.5k_y) \qquad k_x = k_y = G_m(0.1941 + 0.004064M) + 0.01864 \qquad (\mathrm{W\ m^{-1}\ K^{-1}}) \tag{25}$$

The heat of vaporization data from the steam tables are curve fitted using a polynomial as a function of temperature[14] and given as

$$\Delta h_v = 2.792 \times 10^6 - 160T - 3.43T^2 \qquad (\mathrm{J/kg}) \tag{26}$$

The other transport and physical properties used are summarized in Table 1.

Numerical Solution

Equations 15 to 19 are solved numerically using the commercial package Femlab®.[22] This software is used to solve systems of coupled nonlinear and time-dependent PDEs in one, two, or three dimensions.

Equations 15 and 16 can be written in the following generalized form:

$$A_{11}\frac{\partial M}{\partial t} + A_{12}\frac{\partial T}{\partial t} = \vec{\nabla} \cdot [K_{11}\vec{\nabla}M + K_{12}\vec{\nabla}T] \tag{27}$$

$$A_{21}\frac{\partial M}{\partial t} + A_{22}\frac{\partial T}{\partial t} = \vec{\nabla} \cdot [K_{21}\vec{\nabla}M + K_{22}\vec{\nabla}T] \tag{28}$$

where the A_{ij} and K_{ij} coefficients are

$$A_{11} = \rho_d \qquad A_{12} = 0 \qquad A_{21} = 0 \qquad A_{22} = (\rho C_p)_{eff}$$

$$K_{11} = D_M \qquad K_{12} = D_T \qquad K_{21} = k_M \qquad K_{22} = k_{eff} \tag{29}$$

The problem is highly nonlinear because of the temperature and moisture content dependency of the coefficients K_{11}, K_{12},

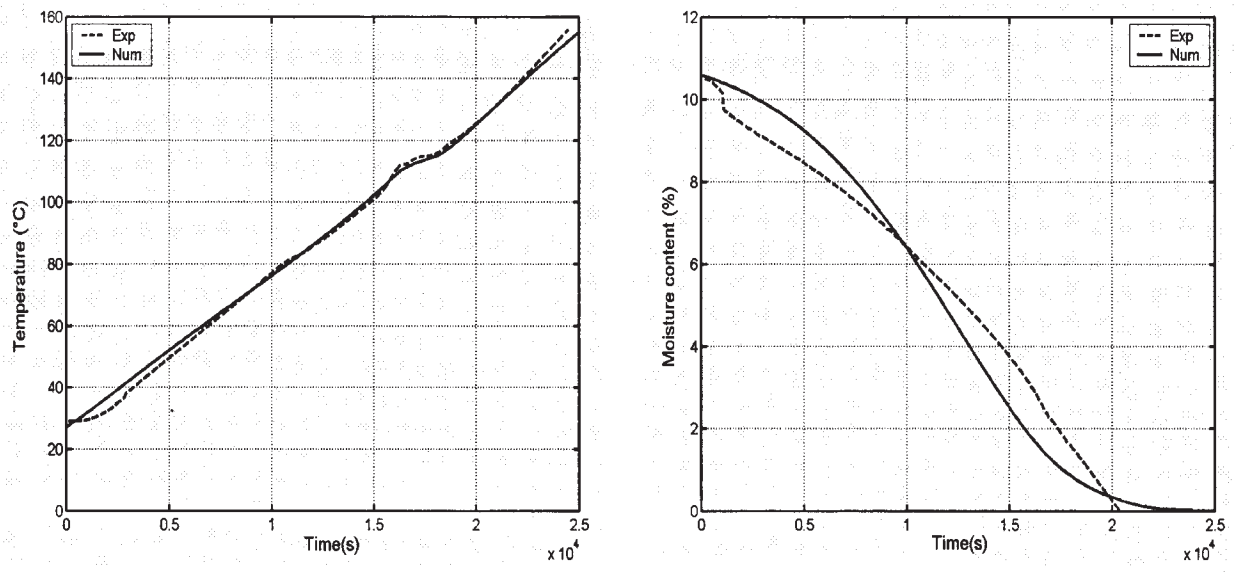

a) $T_{g,final}$=160°C, Heating Rate 20°C/h, M_0=10.59%

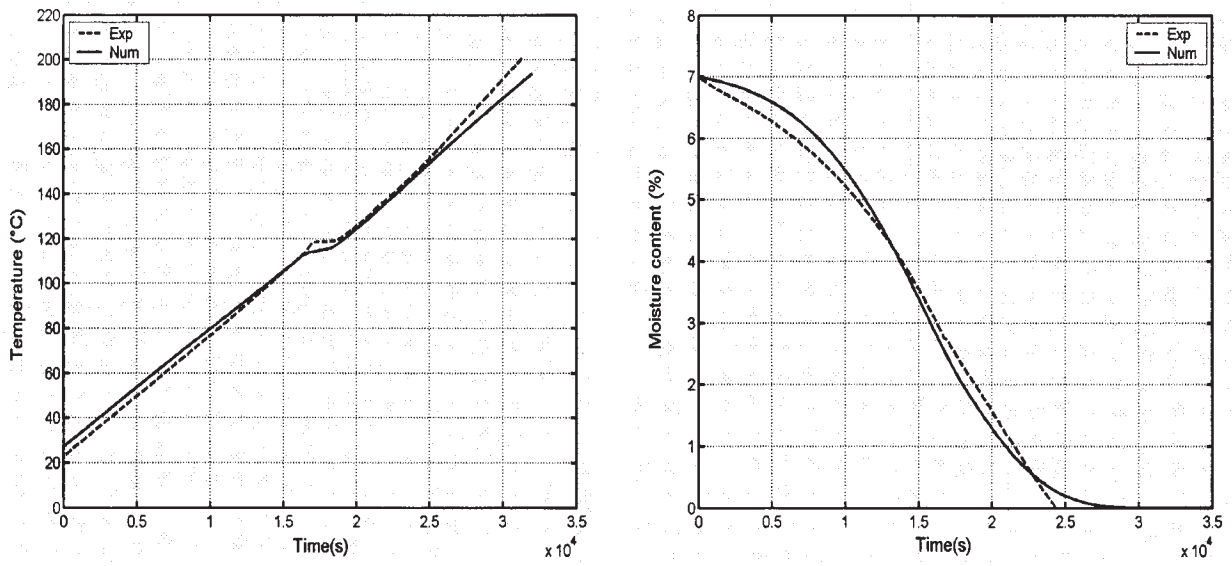

b) $T_{g,final}$=200°C, Heating Rate 20°C/h, M_0=7%

Figure 2. Comparison of predicted and experimental temperature evolution (left) and average moisture content evolution (right) during heat treatment for different final temperatures.

(a) $T_{g,final}$ = 160°C; (b) $T_{g,final}$ = 200°C.

K_{21}, and K_{22} (Appendix A). These coefficients are evaluated at each time step.

Numerical tests were conducted using different time steps and mesh sizes to verify the convergence of the model. For the time steps of 500, 1000, and 3600 s, the differences in temperatures and the moisture contents were found to be <0.5%. The mesh convergence was verified with refined mesh sizes. Consequently, a time step of 500 s and a mesh consisting of 1466 nodes and 6580 elements were used in subsequent simulations.

Results and Discussion

Validation of the mathematical model was carried out by comparing the predictions of the model with the experimental results obtained during the high-temperature treatment of birch. More detailed information on the experimental procedure and the conditions of the base case are given elsewhere.[23] The temperature and moisture evolution data were obtained by heat treating the samples in a thermogravimetric analyzer for different final temperatures (160–220°C) and heating rates (10,

20, and 30°C/h). Dimensions of the samples were 0.035 × 0.035 × 0.2 m. Each sample was air dried before the treatment and had an initial temperature of 25°C. They had slightly different initial moisture contents (7–13%), and this is indicated on each figure. The thermophysical properties and the treatment conditions used in the simulations are listed in Table 1.

The temperature field evolution within the wood has a considerable influence on the treatment and, consequently, on the product quality.

The calculated average moisture contents and temperatures are compared with the experimental data at the reference point $x = 1.27$ cm, $y = 1.75$ cm, $z = 10$ cm for different final treatment temperatures (160 and 200°C); the results are presented in Figure 2. The initial moisture content of each sample was slightly different because of the nonhomogeneous nature of wood, and these are indicated on the figures. It can be clearly seen that a satisfactory agreement between the model results and experimental data is obtained that justifies the basic assumptions of the model. The maximum difference between the model predictions and the experimental data is less than 4 and 10% for the temperature and moisture content distributions, respectively.

During the heat treatment, the temperature increases and the average moisture content decreases almost linearly with time except at later times where the rate of moisture content decrease slows down. This linearity is attributed to the influence of gas temperature, which was also increased linearly with time. There is a short period during which the temperature of the gas is kept constant at 120°C. After this period, the temperature increases until the final treatment temperature is reached at a given heating rate. The heat supplied by the hot gas is used both to evaporate the moisture and to heat the wood. The wood temperature affects the internal moisture transport coefficients as well as the amount of equilibrium moisture content at the solid surface.

The water migrates toward the external wood surfaces by means of capillary flow under the influence of moisture content gradient. The average moisture content approaches zero at the end of treatment. The discrepancies observed between the model predictions and the experimental data might arise from the release of extractable components and the chemical reactions such as the decomposition of hemicelluloses to the water-soluble polymers, which are neglected by the model.

Figure 3 compares the model predictions with the experimental results at heating rates of 10, 20, and 30°C/h, respectively. As can be seen from this figure, the model successfully predicts the behavior of wood during the treatment. As the heating rate decreases, it takes longer to reach a given temperature and to reduce the moisture content to minimum. For all three experiments, the moisture is totally eliminated before the final temperature is reached. It can be observed from the figures that, at any given time, the higher the heating rate, the higher the wood temperature and the lower the average moisture content of the wood. This is expected because higher heating rates result in larger exchange potentials (gradient) between the hot gas and the wood sample, which favors the evaporation of water from wood. At high temperatures, the chemical reactions cause an additional weight loss as a result of the evacuation of volatiles and other degradation products. This phenomenon is not taken into account in the present mathematical model. Therefore, given the exothermic nature of these reactions, the experimentally measured temperatures are slightly higher than those predicted by the model.

It is difficult to experimentally measure the moisture distribution within a sample. As explained previously, only the change in average moisture content with time is measured and compared with the experimental data. Even though the moisture distribution predicted by the model cannot be compared with the experimental results because of the lack of data, the temperature distribution and the average moisture content seem to be predicted successfully by the model. Also, the tendencies observed in the predicted moisture content profiles seem to be reasonable, as can be seen in Figure 4. In this figure, the temperature and moisture content distributions in the x-direction at the central plane of the sample are presented. The heating rate was taken as 20°C/h and the initial moisture content of the sample was 12.5%. At a given position in wood, the temperature increases and the moisture content decreases with time. The temperatures at the boundary surfaces are slightly higher than those at the interior of wood at different

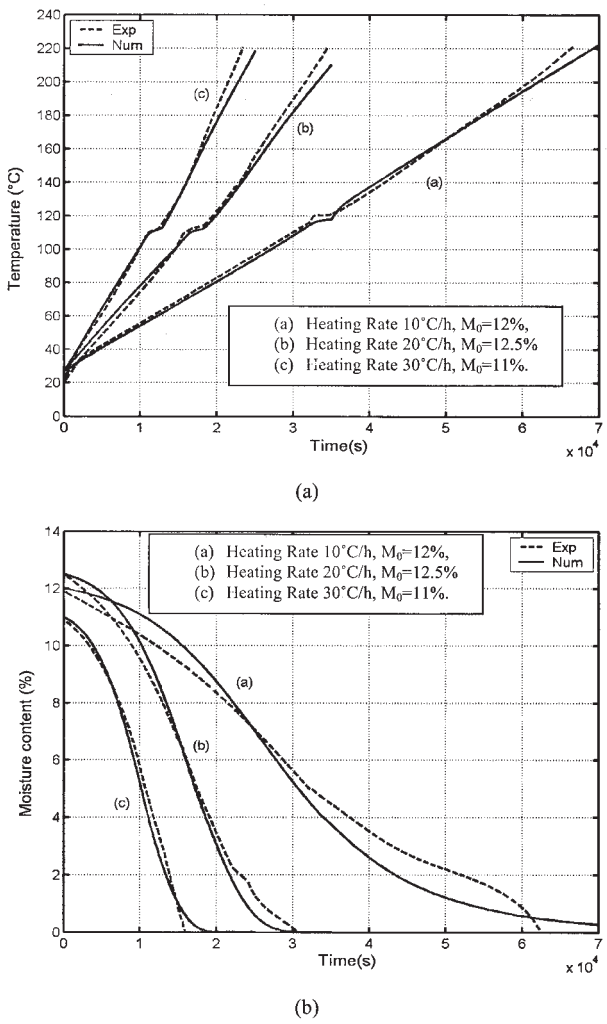

Figure 3. Comparison of predicted and experimental (a) temperature and (b) average moisture content evolutions during heat treatment for different heating rates.

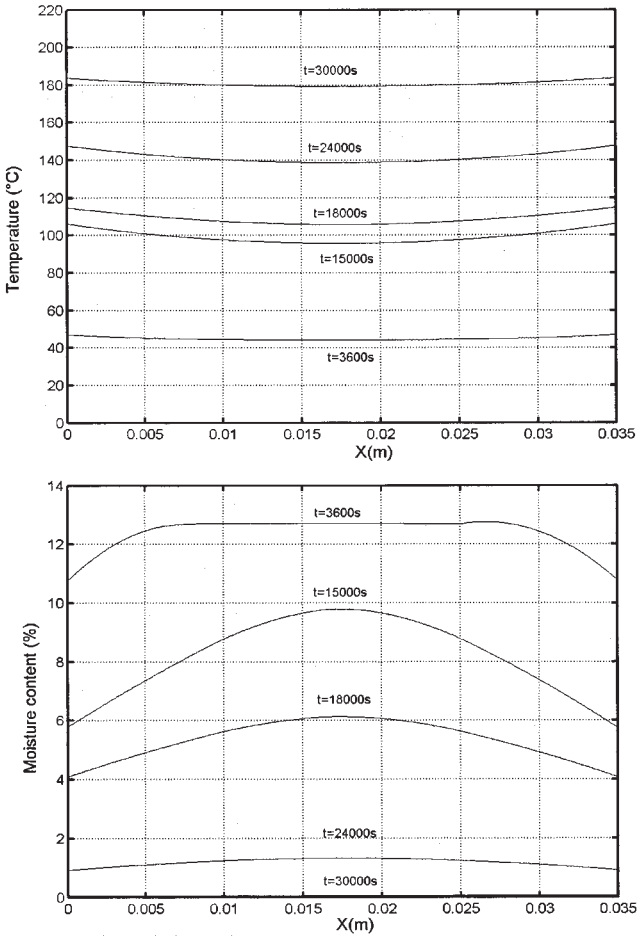

Figure 4. Spatial profiles of (a) temperature and (b) moisture content during heat treatment.

Y = 0.0175 m, Z = 0.1 m, $T_{g,\text{final}}$ = 220°C, heating rate 20°C/h, M_0 = 12.5%.

times. The heated gas stream is the only heat source and is in contact with the wood at the surfaces. The heat is transferred slowly from the surface to the interior of wood because of the low thermal conductivity of wood. The moisture gradient at the surface is very sharp at earlier times and decreases with time. The moisture removal starts at the surface when the hot gas and the wood are in contact. Once the moisture content at the surface of the sample drops, liquid moisture diffuses from the interior parts of the sample to the surface. In the interior parts of the sample, the moisture content is constant at earlier times. As the heating further progresses, the difference between the moisture contents at the surface and in the interior of the sample decreases. All the profiles are symmetrical, as expected, because all external surfaces of the sample are subjected to the same boundary conditions.

The current mathematical model can also be used to predict the effect of different operating parameters on the heat treatment process. Therefore a parametric study was conducted to determine the effects of initial moisture content and sample size on the heat treatment.

A number of simulations were carried out at different initial average moisture contents (M_0) of 10, 20, 30, and 50%, keeping the other conditions constant. The heating rate was maintained at 20°C/h and the final gas temperature was taken as 220°C. Figure 5 shows the predicted temperature and reduced average moisture content (ratio of moisture content at any given time to initial moisture content) as a function of time for various initial moisture contents.

When the initial moisture content is high, the temperature rise is relatively small and drying takes longer. The lower the initial moisture content of the sample, the higher the temperature. This can be explained by the fact that more of the supplied heat is used for the evaporation of water when the moisture content is high, resulting in a slower temperature increase compared to that of samples with lower initial moisture contents. As expected, the reduced average moisture content decreases with time. Under the same treatment conditions, the time necessary for moisture removal is greater when the initial moisture content of the sample is higher.

The influence of sample size on predicted temperatures at the center of the sample is presented in Figure 6a. Simulations were carried out for three different sample sizes. The length of the sample was kept constant (0.2 m). All the

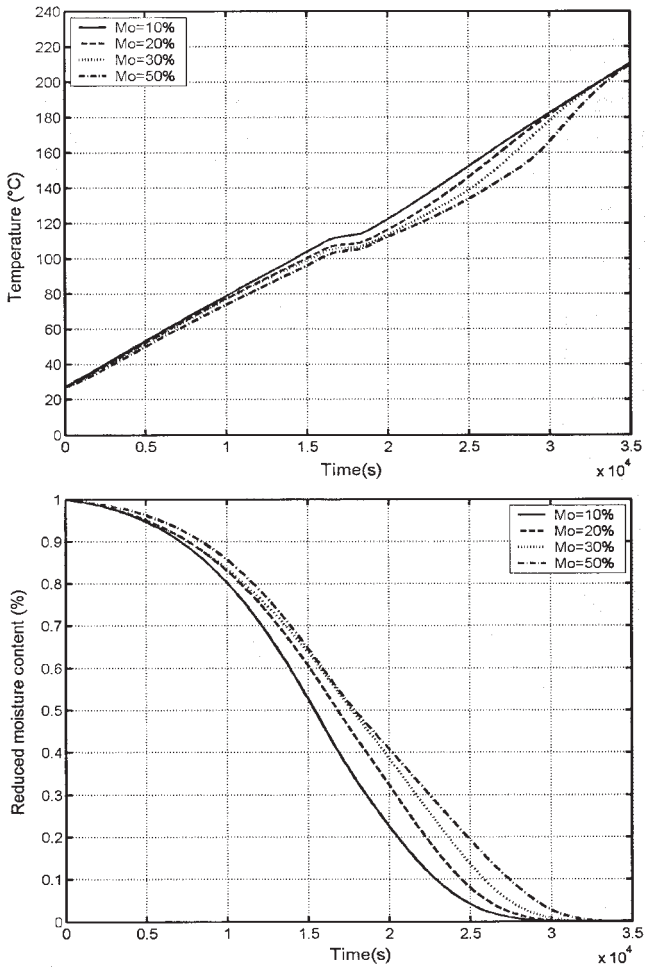

Figure 5. (a) Predicted temperature profiles and (b) predicted average moisture content profiles for different initial wood moisture contents during heat treatment.

$T_{g,\text{final}}$ = 220°C, heating rate 20°C/h.

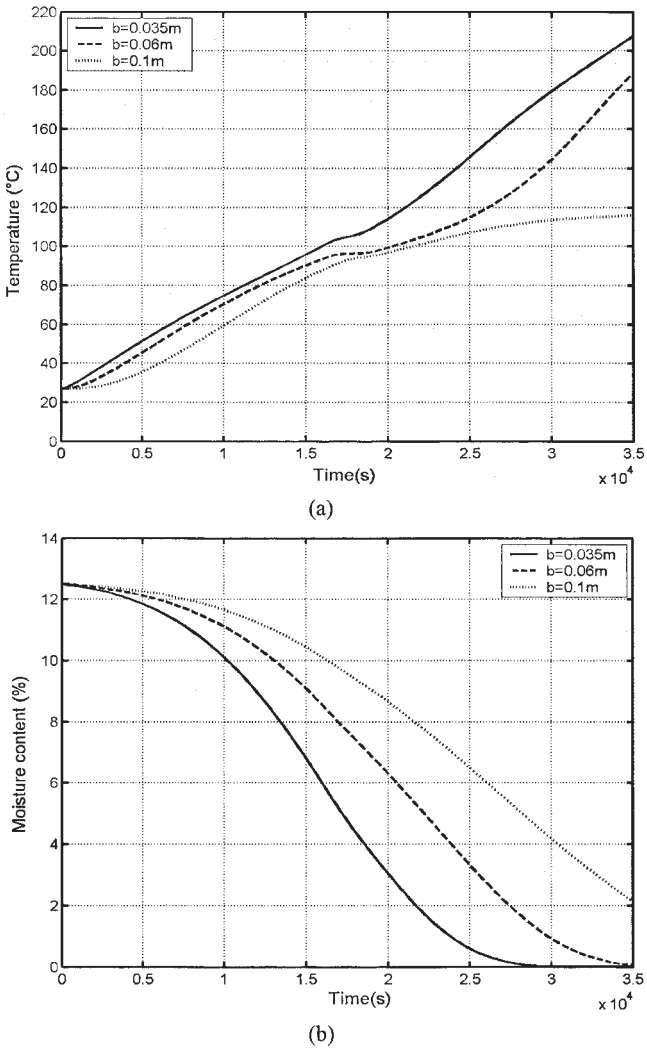

Figure 6. (a) Predicted temperature evolution at center of the wood sample and (b) predicted average moisture content evolution for different wood thicknesses during heat treatment.

$T_{g,\text{final}}$ = 220°C, heating rate 20°C/h, M_0 = 12.5%.

samples had square cross sections. The width and the thickness of the samples were taken as 0.035, 0.06, and 0.1 m. As expected, when the sample size increases, the wood temperature rises at a lower rate, and the time required for the treatment becomes longer as a result of the low thermal conductivity of the wood. The effect of sample size and the differences in the temperatures are clearly seen in this figure.

Figure 6b shows the variation of average moisture content with time for the three samples. It is clear that average moisture content decreases at a faster rate as the sample thickness decreases. To drive the moisture out of the sample, the moisture present in the interior part of the sample has to diffuse to the surface. The evaporation of moisture takes place from the wood surface when the necessary heat (heat of vaporization) is supplied by the hot gas. As the sample size increases, the diffusion process takes longer, thus leading to samples with different final moisture contents, under the same heat treatment conditions.

Conclusions

A general mathematical model has been developed to achieve a better understanding of the high-temperature heat treatment of wood and to determine its influence on several parameters that control the process. Femlab® software was used to solve the system of partial differential equations.

The model predictions are in good agreement with the results of the experiments. There is some difference between the predicted and the measured results for moisture content at the end of the process, which might be attributable to the chemical reactions taking place in the wood at high temperatures. The effects of these reactions on the heat treatment process were outside the scope of this study. However, the model gives all the trends observed experimentally and can be used as an effective tool to predict moisture and temperatures distributions for the high-temperature thermal treatment of wood.

The main difficulty encountered is the availability of accurate data for the thermophysical properties of wood needed for the simulations. Based on the results of this study, it can be stated that the model predicts the behavior of the wood sample during the high-temperature treatment with sufficient accuracy within the range of temperatures considered. This model can also be used for conventional drying (the moisture content above the fiber saturation point).

Not many experimental investigations on the high-temperature thermal treatment of wood are yet available. Further experimental work needs to be done to investigate the chemical reactions and to determine various properties for different wood species. The current model can then be further improved to account for all the phenomena including the reactions.

Acknowledgments

The authors thank the University of Quebec at Chicoutimi (UQAC), the Foundation of the University (FUQAC), the Consortium de recherche sur la forêt boréale commerciale, and especially Dr. Rejean Gagnon and Sylvain Tremblay for their support and contributions.

Notation

b = thickness of the sample, m
C_p = heat capacity, J kg^{-1} K^{-1}
D = diffusion coefficient, m^2 s^{-1}
h = convective heat transfer coefficient, W m^{-2} K^{-1}
h_m = convective mass transfer coefficient, m s^{-1}
$\mathbf{J}$ = vector of total moisture flux, kg m^{-2} s^{-1}
k = thermal conductivity, W m^{-1} K^{-1}
K = permeability, m^2
M = moisture content, kg H_2O/(kg solid)$^{-1}$
m_v = molar mass, kg mol^{-1}
n = normal
Nu = Nusselt number
P = partial water vapor pressure in wood, Pa
P_c = capillary pressure in wood, Pa
P_{sv} = saturation water vapor pressure in wood, Pa
Pr = Prandtl number
Q = heat transfer
Re = Reynolds number
R = ideal gas constant, J mol^{-1} K^{-1}
S = saturation
Sc = Schmidt number
Sh = Sherwood number
t = time, s

T = temperature, K
W = weight, kg

Greek letters

α = coefficient in calculating capillary pressure
β = coefficient in calculating capillary pressure
δ = attenuation factor in the effective diffusivity
ε = void fraction
λ = thermal conductivity, W m^{-1} K^{-1}
μ = dynamic viscosity, kg m^{-1} s^{-1}
μ_b = chemical potential for bound water
φ = relative humidity of the drying gas
ρ = dry body density, kg m^{-3}
Ψ = coefficient for partial pressure of water vapor in wood

Subscripts

0 = initial
b = bound
f = free water
final = final
FSP = fiber saturation point(s)
g = gas
l = liquid
v = vapor

Literature Cited

1. Pang S. Relative importance of vapour diffusion and convective flow in modelling of softwood drying. *Drying Technol.* 1998;16:271-281.
2. Pang S, Langrish TAG, Keey RB. Moisture movement in softwood timber at elevated temperatures. *Drying Technol.* 1994;12:1897-1914.
3. Fhyr C, Rasmuson A. Some aspects of the modelling of wood chips drying in superheated steam. *Int J Heat Mass Transfer.* 1997;40:2825-2842.
4. Johanson A, Fhyr C, Rasmuson A. High temperature convective drying of wood chips with air and superheated steam. *Int J Heat Mass Transfer.* 1997;40:2843-2858.
5. Luikov AV. Systems of differential equations of heat and mass transfer in capillary-porous bodies. *Int J Heat Mass Transfer.* 1975;18:1-14.
6. Luikov AV. *Heat and Mass Transfer*. Moscow, Russia: Mir; 1980.
7. Whitaker S. Simultaneous heat, mass and momentum transfer in porous media: A theory of drying. *Adv Heat Transfer.* 1977;13:119-203.
8. Lewis RW, Morgan K, Thomas HR. *The Finite Element Method in Heat Transfer Analysis*. New York, NY: Wiley; 1996.
9. Malan AG, Lewis RW. Modelling coupled heat and mass transfer in drying non-hygroscopic capillary particulate materials. *Comput Num Methods Eng.* 2003;19:669-677.
10. Gawin D, Majorana CE, Schrefler BA. Numerical analysis of hygrothermal behaviour and damage of concrete at high temperature. *Mech Cohes-Frict Mater.* 1999;4:37-74.
11. Bear J, Bachmat Y. *Introduction to Modelling of Transport Phenomena in Porous Media*. Dordrecht, The Netherlands: Kluwer Academic; 1990.
12. Hassanizadeh M, Gray WG. General conservation equations for multiphase systems. 1. Averaging technique. *Adv Water Res.* 1979;2:131-144.
13. Bories SA. Fundamentals of drying of capillary-porous bodies. In: Kakac S, Kilkis B, Kulacki FA, Arinc F, eds. *Convective Heat and Mass Transfer in Porous Media*. Dordrecht, The Netherlands: Kluwer Academic; 1991.
14. Stanish MA, Schajer GS, Kayihan F. A mathematical model of drying for hygroscopic porous media. *AIChE J.* 1986;32:1301-1311.
15. Moyne C. *Contribution à l'étude du transfert simultané de chaleur et de masse lors du séchage sous vide d'un bois résineux*. PhD Thesis. Nancy, France: Nancy University; 1982.
16. Siau JF. *Transport Processes in Wood*. New York, NY: Springer-Verlag; 1984.
17. Spolek GA, Plumb OA. Capillary pressure in softwoods. *Wood Sci Technol.* 1981;15:189-199.
18. Pakowski Z, Bartczak Z, Strumillo C, Strenstrom S. Evaluation of equations approximating thermodynamic and transport properties of water, steam and air for use in cad of drying process. *Drying Technol.* 1991;9:753-773.
19. Simpson W, Tenwold A. Physical properties and moisture relations of wood. *Wood Handbook*. Madison, WI: USDA Forest Service, Forest Product Laboratory; 1999;3:1-23.
20. Incropera, FP, DeWitt DP. *Fundamentals of Heat and Mass Transfer*. New York, NY: Wiley; 2002.
21. Leon G, Cruz-de-Leon J, Villaseno L. Thermal characterisation of pine wood by photoacoustic and photothermal techniques. *Holz Roh Werkstoff.* 2000;58:241-246.
22. Femlab® 2.0. *Reference Manual*. Burlington, MA: Comsol Inc.; 2000.
23. Younsi R, Kocaefe D, Poncsak S, Kocaefe Y. Thermal modeling of the high temperature treatment of wood based on Luikov's approach. *Int J Energy Res.* 2005;29:000-000.

Appendix A: Diffusion Coefficients

$$D_M = \underbrace{\frac{1.2146 \times 10^{-4} m_v \delta(T)^{0.75}}{R} P_{sv} \frac{\partial \Psi}{\partial M}}_{\text{Vapour term}} + \underbrace{8.314 \frac{\mathrm{D_b}}{\mathrm{m}_v} \frac{\mathrm{T}}{\Psi} \frac{\partial \Psi}{\partial \mathrm{M}}}_{\text{Bound term}} + \underbrace{\frac{\alpha \beta \mathrm{K_l} \rho_\mathrm{l} (\mathrm{M_{max}} - M_{\mathrm{FSP}})^{\beta}}{\mu_l (M - M_{\mathrm{FSP}})^{(1+\beta)}}}_{\text{Free water term}}$$

$$D_T = \underbrace{\frac{1.2146 \times 10^{-4} m_v \delta(T)^{0.75}}{R} \left(\frac{\partial P_{sv}}{\partial T} \Psi + P_{sv} \frac{\partial \Psi}{\partial T} \right)}_{\text{Vapour term}}$$

$$\underbrace{- \frac{D_b}{m_v} \left\{ \left[187 + 35.1 \ln\left(\frac{T}{298.15}\right) - 8.314 \ln\left(\frac{P_v}{101{,}325}\right) \right] - 8.314 \frac{T}{P_v} \left(\frac{\partial P_{sv}}{\partial T} \Psi + P_{sv} \frac{\partial \Psi}{\partial T} \right) \right\}}_{\text{Boundd term}}$$

$$k_{eff} = k + \underbrace{h_v \frac{1.2146 \times 10^{-4} m_v \delta(T)^{0.75}}{R} \left(\frac{\partial P_{sv}}{\partial T} \Psi + P_{sv} \frac{\partial \Psi}{\partial T} \right)}_{\text{Vapour term}}$$

$$\underbrace{- h_b \frac{D_b}{m_v}\left\{\left[187 + 35.1 \ln\left(\frac{T}{298.15}\right) - 8.314 \ln\left(\frac{P_v}{101{,}325}\right)\right] - 8.314 \frac{T}{P_v}\left(\frac{\partial P_{sv}}{\partial T}\Psi + P_{sv}\frac{\partial \Psi}{\partial T}\right)\right\}}_{\text{Bound term}}$$

$$k_M = h_v \underbrace{\frac{1.2146 \times 10^{-4} m_v \delta (T)^{0.75}}{R} P_{sv} \frac{\partial \Psi}{\partial M}}_{\text{Vapour term}} + h_b \underbrace{8.314 \frac{D_b}{m_v} \frac{T}{\Psi} \frac{\partial \Psi}{\partial M}}_{\text{Bound term}} + h_f \underbrace{\frac{\alpha \beta K_l \rho_l (M_{\max} - M_{\text{FSP}})^{\beta}}{\mu_l (M - M_{\text{FSP}})^{(1+\beta)}}}_{\text{Free water term}}$$

$$(\rho C_p)_{eff} = (\rho C_p)_d + (\rho C_p)_v + (\rho C_p)_b + (\rho C_p)_f$$

Appendix B

Table B1. Transport Property Equations*

	Coefficient				
	a_0	a_1	a_2	a_3	a_4
$Cp_l = \sum_{i=0}^{n} a_i T(K)^i$	2.8223	1.1828E-2	−3.5047E-5	3.6010E-8	
$Cp_v = \sum_{i=0}^{n} a_i T(K)^i$	1.8830	−0.1674E-3	0.8439E-6	−0.2697E-9	
$h_l = \sum_{i=0}^{n} a_i T(K)^i$	−7.8955E5	−4.476206E2	2.274399E1	−4.9553577E-2	4.041035E-5
$h_v = \sum_{i=0}^{n} a_i T(K)^i$	1.891879E6	2.56352E3	−1.2360577		
$\rho_l = \sum_{i=0}^{n} a_i T(K)^i$	961.12885	0.3703	−2.38654E-4	−2.06894E-6	
$\mu_l = \sum_{i=0}^{n} a_i T(K)^i$	0.44576	−0.00515	2.24414E-5	−4.35692E-8	3.17749E-11

*From Pakowski et al.[18].

Appendix C: Equilibrium Moisture Content

Coefficients used in the governing equations for the high-temperature heat treatment of wood are given in the following list:

$$M_{eq} = \frac{18}{w}\left(\frac{k_1 k_2 \varphi}{1 + k_1 k_2 \varphi} + \frac{k_2 \varphi}{1 - k_2 \varphi}\right)$$

$$k_1 = 4.737 + 0.4773T - 0.000500012T^2$$

$$k_2 = 0.7059 + 0.001695T - 0.00005638T^2$$

$$w = 223.4 + 0.6942T + 0.01853T^2$$

Manuscript received Nov. 17, 2005, and revision received Mar. 6, 2006.